

Phase diagrams of forced magnetic reconnection in Taylor's model

L. Comisso^{1,2,†,‡}, D. Grasso^{1,2} and F. L. Waelbroeck³

¹Dipartimento Energia, Politecnico di Torino, Corso Duca degli Abruzzi 24, Torino 10129, Italy

²Istituto dei Sistemi Complessi – CNR, Via dei Taurini 19, Roma 00185, Italy

³Institute for Fusion Studies, The University of Texas at Austin, Austin, TX 78712-1203, USA

(Received 30 April 2015; revised 8 June 2015; accepted 9 June 2015)

Recent progress in the understanding of how externally driven magnetic reconnection evolves is organized in terms of parameter space diagrams. These diagrams are constructed using four pivotal dimensionless parameters: the Lundquist number S , the magnetic Prandtl number P_m , the amplitude of the boundary perturbation $\hat{\psi}_0$, and the perturbation wave number \hat{k} . This new representation highlights the parameter regions of a given system in which the magnetic reconnection process is expected to be distinguished by a specific evolution. Contrary to previously proposed phase diagrams, the diagrams introduced here take into account the dynamical evolution of the reconnection process and are able to predict slow or fast reconnection regimes for the same values of S and P_m , depending on the parameters that characterize the external drive, which have not been considered until now. These features are crucial to understanding the onset and evolution of magnetic reconnection in diverse physical systems.

1. Introduction

Magnetic reconnection is a process whereby the magnetic field line connectivity (Newcomb 1958; Pegoraro 2012; Asenjo & Comisso 2015) is modified due to the presence of a localized diffusion region. This gives rise to a change in magnetic field line topology and a release of magnetic energy into kinetic and thermal energy. Reconnection of magnetic field lines is ubiquitous in laboratory, space and astrophysical plasmas, where it is believed to play a key role in many of the most striking and energetic phenomena. The most notable examples of such phenomena include sawtooth crashes (Yamada *et al.* 1994; Nicolas *et al.* 2012) and major disruptions in tokamak experiments (Waddell *et al.* 1978; Boozer 2012), solar and stellar flares (Masuda *et al.* 1994; Su *et al.* 2013), coronal mass ejections (Lin & Forbes 2000; Murphy *et al.* 2012), magnetospheric substorms (Øieroset *et al.* 2001; Eastwood *et al.* 2007), coronal heating (Priest *et al.* 1998; Cassak *et al.* 2008), and high-energy emissions in pulsar wind nebulae, gamma-ray bursts and jets from active

† Email address for correspondence: luca.comisso@polito.it

‡ Contributed talk at the International Workshop 'Complex Plasma Phenomena in the Laboratory and in the Universe'.

galactic nuclei (Guo *et al.* 2015; Kagan *et al.* 2015; Sironi *et al.* 2015). An exhaustive understanding of how magnetic reconnection proceeds in various regimes is therefore essential in order to shed light on these phenomena.

In recent years, for the purpose of organizing the current knowledge of the reconnection dynamics that is expected in a system with given plasma parameters, a particular type of phase diagrams has been developed (Huang *et al.* 2011; Ji & Daughton 2011; Daughton & Roytershteyn 2012; Cassak & Drake 2013; Huang & Bhattacharjee 2013; Karimabadi & Lazarian 2013). These diagrams classify what ‘phase’ of magnetic reconnection should occur in a particular system, which is identified by two dimensionless plasma parameters, the Lundquist number

$$S_{L_s} \equiv \frac{L_s v_{A,u}}{D_\eta}, \quad (1.1)$$

and the macroscopic system size

$$\Lambda \equiv \frac{L_s}{l_k}. \quad (1.2)$$

Here, L_s indicates the system size in the direction of the reconnecting current sheet, $v_{A,u}$ is the Alfvén speed based on the reconnecting component of the magnetic field upstream of the diffusion region, $D_\eta = \eta c^2 / 4\pi$ is the magnetic diffusivity, and l_k is the relevant kinetic length scale. This length scale corresponds to (see e.g. Simakov & Chacón 2008; Comisso *et al.* 2013)

$$l_k = \begin{cases} d_i = c / \omega_{pi} & \text{for antiparallel reconnection,} \\ \rho_\tau = c_s / \omega_{ci} & \text{for guide-field reconnection.} \end{cases} \quad (1.3)$$

Of course, ω_{pi} is the ion plasma frequency, ω_{ci} is the ion cyclotron frequency, c is the speed of light, and c_s is the sound speed based on both the electron and ion temperatures.

All the proposed phase diagrams (Huang *et al.* 2011; Ji & Daughton 2011; Daughton & Roytershteyn 2012; Cassak & Drake 2013; Huang & Bhattacharjee 2013; Karimabadi & Lazarian 2013) exhibit strong similarity and only a few minor differences. They are useful for summarizing some of the current knowledge of the magnetic reconnection dynamics, but they lack fundamental aspects that can greatly affect the reconnection process (some caveats in the use of these diagrams have been discussed by Cassak & Drake 2013). For example, they do not take into account the dependence of the reconnection process on the external drive or on the magnetic free energy available in the system. An attempt to include these effects has been discussed by Ji & Daughton (2011), who proposed incorporating them by adjusting the definition of the Lundquist number (1.1), but this solution should be viewed only as a rough way to circumnavigate the problem. A further issue is that these diagrams do not consider the evolution of the reconnection process, and predict reconnection rates which are always fast (the estimated reconnection inflow is always a significant fraction of $v_{A,u}$). This, however, is not what is commonly observed in laboratory, space, and astrophysical plasmas, where magnetic reconnection exhibits disparate time scales and is often characterized by an impulsive behaviour, i.e. a sudden increase in the time derivative of the reconnection rate (see e.g. Bhattacharjee 2004; Yamada 2011).

Here we propose a different point of view in which we include explicitly the effects of the external drive and the plasma viscosity (neglected in all previous diagrams) on the magnetic reconnection process by considering a four-dimensional parameter space. Then, in this four-dimensional diagram we identify specific domains of parameters where the reconnection process exhibits distinct dynamical evolutions. In other words, in each of these domains the reconnection process goes through diverse phases characterized by different reconnection rates. This analysis leads us to evaluate in greater detail the dynamical evolution of a forced magnetic reconnection process, while collisionless effects have not been taken into account in the present work. We introduce the considered model of forced magnetic reconnection in §2, whereas §3 is devoted to the presentation of the possible evolutions of the system and the conditions under which these different evolutions occur. In §4 we construct the parameter space diagrams that show which reconnection evolution is expected in a system with given characteristic parameters. Finally, open issues are discussed in §5.

2. Forced magnetic reconnection in Taylor's model

Magnetic reconnection in a given system is conventionally categorized as spontaneous or forced. Spontaneous magnetic reconnection refers to the case in which the reconnection arises by some internal instability of the system or loss of equilibrium, with the most typical example being the tearing mode. Forced magnetic reconnection instead refers to the cases in which the reconnection is driven by some externally imposed flow or magnetic perturbation. In this case, one of the most important paradigms is the so-called 'Taylor problem', which consists in the study of the evolution of the magnetic reconnection process in a tearing-stable slab plasma equilibrium which is subject to a small amplitude boundary perturbation. This situation is depicted in figure 1, where the shared equilibrium magnetic field has the form

$$\mathbf{B} = B_z \mathbf{e}_z + (x/L) B_0 \mathbf{e}_y, \quad (2.1)$$

with B_z , B_0 and L as constants, and the perfectly conducting walls which bound the plasma are located at $x = \pm L$. Magnetic reconnection is driven at the resonant surface $x = 0$ by a deformation of the conducting walls such that

$$x_w \rightarrow \pm L \mp \mathcal{E}_0 \cos(ky), \quad (2.2)$$

where $k = 2\pi/L_y$ is the perturbation wave number and \mathcal{E}_0 is a small ($\ll L$) displacement amplitude. The boundary perturbation is assumed to be set up in a time scale that is long compared to the Alfvén time $\tau_A = L/v_A$, with $v_A = B_0/\sqrt{4\pi\rho}$, but short compared to any characteristic reconnection time scale. Hence, the plasma can be considered in magnetostatic equilibrium everywhere except near the resonant surface at $x = 0$.

The first and probably most important contribution to unveiling the behaviour of forced magnetic reconnection in Taylor's model is due to Hahn & Kulsrud (1985), who showed that very small amplitude boundary perturbations cause an initial linear phase in which a current sheet builds up at the resonant surface, and successive phases in which the reconnection process evolves according to a linear resistive regime and a nonlinear Rutherford regime (Rutherford 1973). The scenario discussed by Hahn & Kulsrud (1985), which is characterized by a very slow evolution of the reconnection process, was complemented some years later by Wang & Bhattacharjee (1992a),

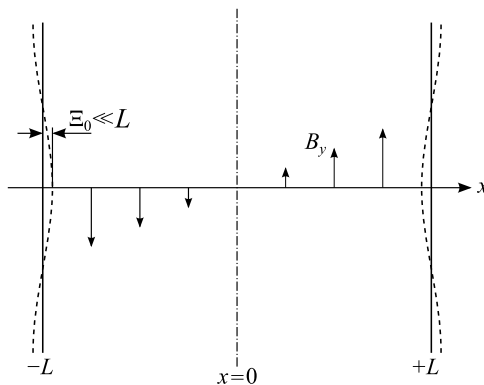


FIGURE 1. Geometry of the Taylor model. The equilibrium magnetic field component B_y is sheared in the x direction, being null at $x = 0$. The plasma is bounded by perfectly conducting walls at $x = \pm L$, while it is periodic in the y direction. Magnetic reconnection is driven at $x = 0$ by the perturbation $\Xi_0 \cos(ky)$ at the perfectly conducting walls.

who showed that larger perturbations may foster reconnection to proceed through the nonlinear regime according to a Sweet–Parker-like evolution (Waelbroeck 1989), which gives way to a Rutherford evolution only on the long time scale of resistive diffusion. The scenario outlined by Wang & Bhattacharjee (1992a) is characterized by a reconnection evolution faster than that presented by Hahn & Kulsrud (1985), but it could still be slow for very small values of plasma resistivity, since in both the Sweet–Parker-like (Waelbroeck 1989) and Rutherford (Rutherford 1973) regimes, the reconnection rate is strongly dependent on the resistivity, which is known to be extremely small in many laboratory fusion plasmas and space/astrophysical plasmas. However, recent works (Comisso *et al.* 2014, 2015) have shown that relatively large boundary perturbations lead to a different reconnection evolution in plasmas with small resistivity and viscosity. In these cases, after a linear inertial phase and an initial nonlinear regime characterized by a gradually evolving current sheet, the reconnection suddenly enters into a fast reconnection regime distinguished by the disruption of the current sheet due to the development of secondary magnetic islands (usually called plasmoids: see Biskamp 2000 or Loureiro *et al.* 2007).

In addition to the works discussed above, which adopt a magnetohydrodynamic (MHD) description of the plasma, we emphasize that many other efforts have been devoted to investigating the Taylor problem assuming MHD, two-fluid and kinetic descriptions (see Wang & Bhattacharjee 1992b; Ma *et al.* 1996; Avinash *et al.* 1998; Rem & Schep 1998; Valori *et al.* 2000; Fitzpatrick 2003; Fitzpatrick 2004a,b, 2008; Fitzpatrick *et al.* 2003; Cole & Fitzpatrick 2004; Bian & Vekstein 2005; Birn *et al.* 2005; Vekstein & Bian 2006; Birn & Hesse 2007; Hosseinpour & Vekstein 2008; Gordovskyy *et al.* 2010a,b; Lazzaro & Comisso 2011; Dewar *et al.* 2013; Hosseinpour 2013). Indeed, the Taylor problem has important applications besides being interesting from the point of view of basic physics. For instance, in laboratory fusion plasmas the Taylor model represents a convenient way to study magnetic reconnection processes driven by resonant magnetic perturbations, while in astrophysical plasmas this model can be adopted to the study of magnetic reconnection forced by the motions of photospheric flux tubes.

3. Evolution of the reconnection process in Taylor's model

In this section we review the present understanding of the forced magnetic reconnection dynamics in Taylor's model focusing on a visco-resistive plasma with P_m greater than 1. As shown by Hahm & Kulsrud (1985), this dynamics always starts with a linear inertial phase in which a current sheet builds up at the resonant surface and shrinks inversely in time. Concurrently, the current density at the X -point increases linearly in time. The reconnection rate during this phase can be evaluated by recalling that the current density is proportional to the out-of-plane electric field at the X -point, which is equal to

$$\partial_t \psi|_X = \frac{2}{\pi} \Delta'_s k L^2 B_0 \mathcal{E}_0 \frac{t}{\tau_A \tau_\eta} \quad (3.1)$$

for $t \ll \tau_v^{1/3} (\tau_A/kL)^{2/3}$ (Fitzpatrick 2003; Comisso *et al.* 2015). Here, ψ stands for the magnetic flux function of the perturbed magnetic field in the reconnection plane ($\delta \mathbf{B}_\perp = \nabla \psi \times \mathbf{e}_z$), $\tau_v = L^2/\nu$ and $\tau_\eta = L^2/D_\eta$ indicate the characteristic time for viscous and resistive diffusion, respectively, while $\Delta'_s = 2k/\sinh(kL)$ parametrizes the contribution of the external source perturbation to the gradient discontinuity of the magnetic flux function at the resonant surface. It is important to point out that this phase is characterized by a non-constant- ψ behaviour of the magnetic flux function across the island. Depending on whether or not this property persists until the beginning of the nonlinear regime, different scenarios may occur.

3.1. Hahm–Kulsrud scenario

If the boundary perturbation is such that (Fitzpatrick 2003; Comisso *et al.* 2015)

$$\Psi_0 = B_0 \mathcal{E}_0 \ll (\tau_v \tau_\eta)^{-1/6} \left(\frac{\tau_A}{kL} \right)^{1/3} \frac{B_0}{\Delta'_s} \equiv \Psi_w, \quad (3.2)$$

after the inertial phase the reconnection process evolves through a visco-resistive phase, which is a linear regime characterized by a constant- ψ behaviour, i.e. the perturbed magnetic flux function can be treated as a constant in x over the width of the reconnection layer. During this phase the reconnection rate is given by

$$\partial_t \psi|_X = B_0 \mathcal{E}_0 \frac{\Delta'_s L}{\tau_*} e^{\Delta'_s L t / \tau_*}, \quad (3.3)$$

where $\Delta'_0 = 2k/\tanh(kL)$ is the standard tearing stability parameter and τ_* is a characteristic time defined as (Fitzpatrick 2003; Comisso *et al.* 2015)

$$\tau_* \equiv \pi 6^{2/3} \frac{\Gamma(\frac{5}{6})}{\Gamma(\frac{1}{6})} \frac{\tau_\eta^{5/6}}{\tau_v^{1/6}} \left(\frac{\tau_A}{kL} \right)^{1/3}, \quad (3.4)$$

with Γ indicating the Gamma function. Equation (3.3) is valid for $t \gg \tau_v^{-1/3} \tau_\eta^{2/3} (\tau_A/kL)^{2/3}$ (Fitzpatrick 2003; Comisso *et al.* 2015) and a magnetic island width much smaller than the linear layer width, i.e. $w \ll \delta_{v\eta} \sim (\tau_v \tau_\eta)^{-1/6} (\tau_A/kL)^{1/3} L$ (Porcelli 1987; Fitzpatrick 1993). If the perturbation is sufficient to drive the magnetic island into the nonlinear regime ($w \gtrsim \delta_{v\eta}$), the visco-resistive phase ends up in a Rutherford evolution, whose island width growth is governed by the Rutherford equation

$$\mathcal{I} \frac{\tau_\eta}{L^2} \frac{dw}{dt} = \Delta'_0 + \Delta'_s \frac{\Psi_0}{\psi|_X}, \quad (3.5)$$

where $\mathcal{I} = 0.823$ (Rutherford 1973; Fitzpatrick 1993). This is a very slow reconnection evolution in which the reconnection rate can be evaluated analytically in the two limits (Hahm & Kulsrud 1985; Comisso *et al.* 2015)

$$\partial_t \psi|_X = \frac{2\Delta'_s \Psi_0}{(-\Delta'_0)\tau_{NL}} \left(\frac{3t}{\tau_{NL}}\right)^{-1/3} \quad \text{for } t \ll \tau_{NL}, \tag{3.6}$$

$$\partial_t \psi|_X = \frac{2\Delta'_s \Psi_0}{(-\Delta'_0)\tau_{NL}} \tanh\left(\frac{t}{\tau_{NL}}\right) \cosh^{-2}\left(\frac{t}{\tau_{NL}}\right) \quad \text{for } t \gg \tau_{NL}, \tag{3.7}$$

where

$$\tau_{NL} = \frac{4\mathcal{I}}{(-\Delta'_0)L} \left(\frac{\Delta'_s}{(-\Delta'_0)} \frac{\Xi_0}{L}\right)^{1/2} \tau_\eta. \tag{3.8}$$

3.2. Wang–Bhattacharjee scenario

If the boundary perturbation is such that (Fitzpatrick 2003; Comisso *et al.* 2015)

$$\Psi_0 \gtrsim \Psi_W, \tag{3.9}$$

the non-constant- ψ behaviour characteristic of the inertial phase lingers until the nonlinear regime is entered. Therefore, since in this case the magnetic island grows faster than the current can diffuse out of the reconnecting layer, the evolution of the reconnection process is distinguished by a strong current sheet at the resonant surface (Waelbroeck 1989). The reconnecting current sheet turns out to be stable if the boundary perturbation is such that (Comisso *et al.* 2015)

$$\Psi_0 = B_0 \Xi_0 < CB_0 L \frac{k}{\Delta'_s} \frac{\tau_A}{\tau_\eta} \left(1 + \frac{\tau_\eta}{\tau_\nu}\right)^{1/2} \equiv \Psi_c, \tag{3.10}$$

where the multiplicative constant $C \sim 2\epsilon_c^{-2}$ depends on the critical inverse aspect ratio of the reconnecting current sheet (specified later). In this case, the reconnection process follows a Sweet–Parker evolution (modified by plasma viscosity: Park *et al.* 1984), whose reconnection rate in Taylor’s model is (Comisso *et al.* 2015)

$$\partial_t \psi|_X \approx \frac{1}{3} B_0 L (\Delta'_s \Xi_0)^{3/2} \left(\frac{kL}{\tau_A \tau_\eta}\right)^{1/2} \left(1 + \frac{\tau_\eta}{\tau_\nu}\right)^{-1/4}. \tag{3.11}$$

Finally, the Sweet–Parker type of evolution gives way to a Rutherford evolution on the time scale of resistive diffusion.

3.3. Our scenario

If the boundary perturbation satisfies (Fitzpatrick 2003; Comisso *et al.* 2015)

$$\Psi_0 \gtrsim (\tau_\nu \tau_\eta)^{-1/6} \left(\frac{\tau_A}{kL}\right)^{1/3} \frac{B_0}{\Delta'_s} \equiv \Psi_W \tag{3.12}$$

and also the condition (Comisso *et al.* 2015)

$$\Psi_0 > CB_0 L \frac{k}{\Delta'_s} \frac{\tau_A}{\tau_\eta} \left(1 + \frac{\tau_\eta}{\tau_\nu}\right)^{1/2} \equiv \Psi_c, \tag{3.13}$$

the reconnection process does not reach a stable Sweet–Parker regime, but a different situation occurs. A gradually thinning current sheet evolves until its aspect ratio

reaches the limit that allows the plasmoid instability to develop. The growth of the plasmoids leads to the disruption of the current sheet, and therefore to a dramatic increase in the reconnection rate. The reconnection rate during this plasmoid-dominated phase has been evaluated in a statistical steady state as (Comisso *et al.* 2015)

$$\partial_t \psi_p \approx \epsilon_c B_0 L (\Delta'_s \mathcal{E}_0)^2 \tau_A^{-1} \left(1 + \frac{\tau_\eta}{\tau_v} \right)^{-1/2}, \tag{3.14}$$

where $\epsilon_c = \delta_c/L_c$ is the critical inverse aspect ratio of the reconnecting current sheet. This quantity, whose value has been found to lie in the range 1/100–1/200 by means of numerical simulations (Bhattacharjee *et al.* 2009; Cassak *et al.* 2009; Samtaney *et al.* 2009; Huang & Bhattacharjee 2010; Skender & Lapenta 2010), represents the threshold below which the reconnecting current sheet becomes unstable to the plasmoid instability (Loureiro *et al.* 2007). This threshold condition as a function of the Lundquist and magnetic Prandtl numbers has been recently discussed by Loureiro *et al.* (2013), Comisso *et al.* (2015) and Tenerani *et al.* (2015). In particular, it has been shown (Comisso *et al.* 2015) that a reconnecting current sheet becomes unstable when the Lundquist number based on its length exceeds the critical value $S_c \approx \epsilon_c^{-2} (1 + \tau_v/\tau_\eta)^{1/2}$.

4. Phase diagrams

In this section we illustrate the domain of existence of the three different scenarios described above, with the help of appropriate parameter space maps. For the sake of clarity we restate the three types of reconnection evolutions we are referring to:

- (1) the Hahm–Kulsrud scenario (Hahm & Kulsrud 1985; Fitzpatrick 2003);
- (2) the Wang–Bhattacharjee scenario (Wang & Bhattacharjee 1992*a*; Fitzpatrick 2003);
- (3) our scenario (Comisso *et al.* 2015).

Since each of these scenarios includes different phases/regimes of reconnection, the concept of ‘phase diagrams’ is intended here in a broader sense. Due to this fact, they could also be defined in a more general way as ‘scenario diagrams’. This type of diagrams can be constructed from the conditions summarized in the previous section. Therefore, the possible evolutions of the reconnection process may be organized in a four-dimensional parameter space map with $\hat{\Psi}_0 = \Psi_0/B_0L$, $\hat{k} = kL$, $S = Lv_A/D_\eta$, and $P_m = \nu/D_\eta$ on the four axes. However, due to the difficulty in visualizing such a four-dimensional diagram, it is convenient to consider two-dimensional slices for fixed values of two of the four parameters.

Let us first consider four two-dimensional slices with fixed values of the magnetic Prandtl number and perturbation wave number. Assuming that the Hahm–Kulsrud scenario (which occurs if $\Psi_0 \ll \Psi_w$) holds until $\Psi_0 = \Psi_w/3$, the corresponding diagrams for (a) $\hat{k} = 1/8$, $P_m = 5$, (b) $\hat{k} = 1/8$, $P_m = 500$, (c) $\hat{k} = 2$, $P_m = 5$, and (d) $\hat{k} = 2$, $P_m = 500$ are shown in figure 2(a–d). From these plots it is clear that the Wang–Bhattacharjee scenario is limited to a small range of values of the Lundquist number and the source perturbation amplitude. Increasing values of the magnetic Prandtl number and perturbation wave number extend the domain of existence of this possible type of evolution of the system. However, after a threshold value of the Lundquist number (identified by the intersection of the two black lines representing $\hat{\Psi}_0 = \hat{\Psi}_w/3$ and $\hat{\Psi}_0 = \hat{\Psi}_c$), the Wang–Bhattacharjee scenario cannot occur because

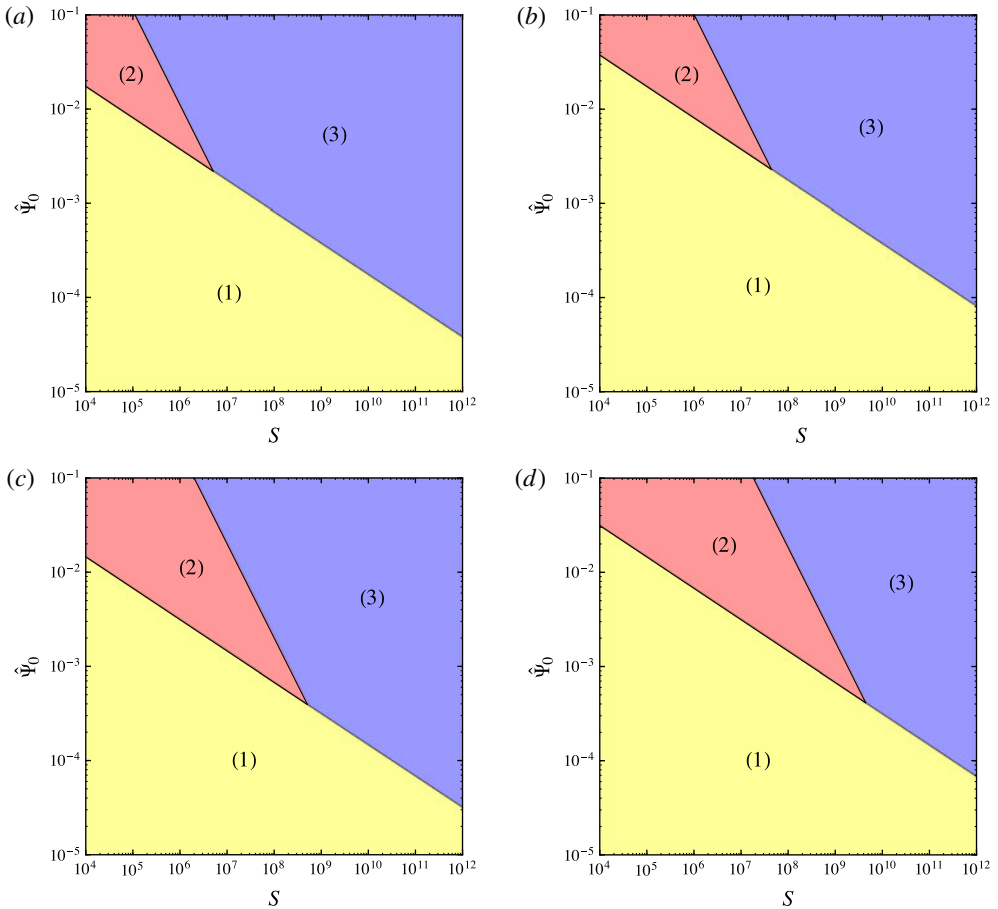


FIGURE 2. Two-dimensional slices of a phase/scenario diagram for forced magnetic reconnection in the magnetohydrodynamical Taylor model. Fixed parameters are (a) $\hat{k} = 1/8$, $P_m = 5$, (b) $\hat{k} = 1/8$, $P_m = 500$, (c) $\hat{k} = 2$, $P_m = 5$, and (d) $\hat{k} = 2$, $P_m = 500$. The numerical labels indicate (1) the Hahm–Kulsrud scenario, (2) the Wang–Bhattacharjee scenario, and (3) our scenario. The boundaries between the different scenarios are identified by the functions $\hat{\Psi}_0 = \hat{\Psi}_w/3$ and $\hat{\Psi}_0 = \hat{\Psi}_c$ for $\hat{\Psi}_c > \hat{\Psi}_w/3$.

it is not possible to obtain a stable Sweet–Parker-type evolution. In these cases the Hahm–Kulsrud scenario is facilitated by very small perturbation amplitudes, whereas larger perturbations lead the system to a fast reconnection regime as described in § 3.3. Note that while previously proposed phase diagrams always predict fast reconnection (Huang *et al.* 2011; Ji & Daughton 2011; Daughton & Roytershteyn 2012; Cassak & Drake 2013; Huang & Bhattacharjee 2013; Karimabadi & Lazarian 2013), in clear contrast to what happens in nature, our diagrams show that reconnection proceeds very slowly (region (1)) if the source perturbation is not sufficiently large.

Let us now examine the effect of the plasma viscosity by considering the domain of existence of the different scenarios as a function of the parameters $\hat{\Psi}_0$ and P_m . Figure 3(a) shows the functions $\hat{\Psi}_0 = \hat{\Psi}_w/3$ and $\hat{\Psi}_0 = \hat{\Psi}_c$ for $S = 10^8$ and $\hat{k} = 0.5$. For $\hat{\Psi}_c < \hat{\Psi}_w/3$ the threshold for plasmoid formation coincides with that for the nonlinear

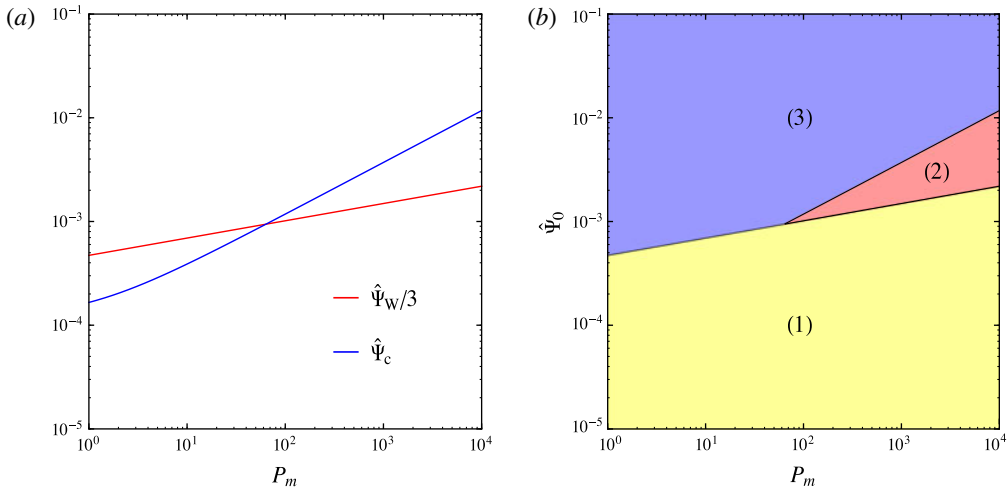


FIGURE 3. (a) Thresholds $\hat{\Psi}_W/3$ (red line) and $\hat{\Psi}_c$ (blue line) as a function of the magnetic Prandtl number P_m for $S = 10^8$, $\hat{k} = 0.5$ and $C = 2(150)^2$. (b) Corresponding two-dimensional slice of the phase/scenario diagram identifying (1) the Hahn–Kulsrud scenario, (2) the Wang–Bhattacharjee scenario, and (3) our scenario.

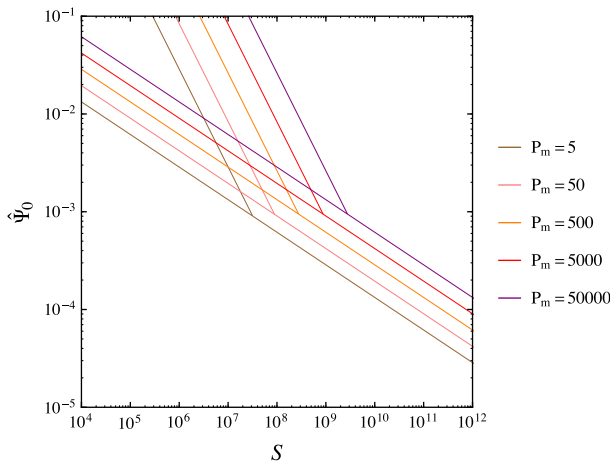


FIGURE 4. Boundaries (identified by the functions $\hat{\Psi}_0 = \hat{\Psi}_W/3$ and $\hat{\Psi}_0 = \hat{\Psi}_c$ for $\hat{\Psi}_c > \hat{\Psi}_W/3$) of the different possible evolutions of the reconnection process for $\hat{k} = 0.5$ and various values of the magnetic Prandtl number.

evolution characterized by a strong reconnecting current sheet. Therefore, for $\hat{\Psi}_c < \hat{\Psi}_W/3$ an increase in the amplitude perturbation $\hat{\Psi}_0$ drives the system directly from scenario (1) to scenario (3). This situation is depicted in figure 3(b), where it is clearly shown that the increase of the magnetic Prandtl number has the effect of making possible or extending the domain of existence of scenario (2), as recently pointed out in Tenerani *et al.* (2015) and Comisso *et al.* (2015).

To clarify the effect of the plasma viscosity we also delineate the boundaries of the diverse evolutions (1)–(3) in a parameter space map $(\hat{\Psi}_0, S)$ (as in figure 2) for fixed $\hat{k} = 0.5$ but different values of P_m . This is shown in figure 4 for $P_m = 5 - 5 \times 10^5$.

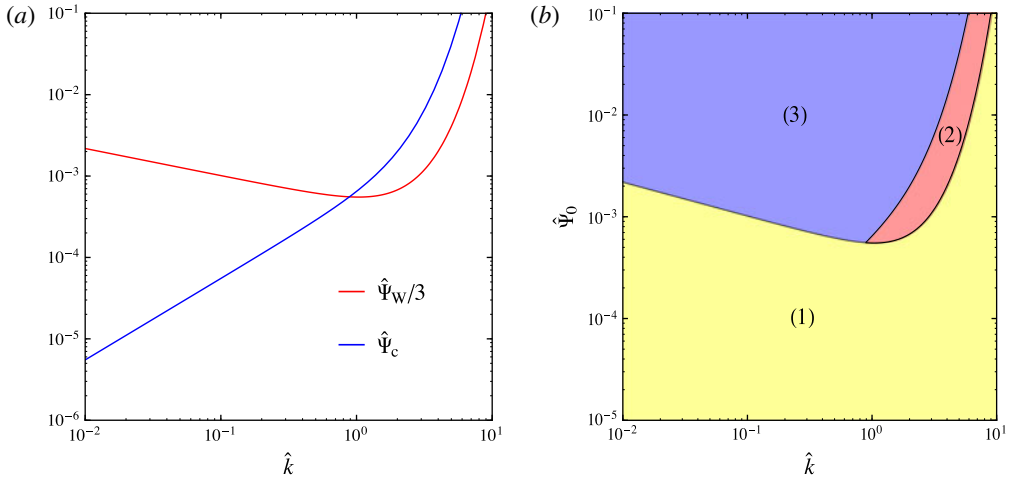


FIGURE 5. (a) Thresholds $\hat{\Psi}_W/3$ (red line) and $\hat{\Psi}_c$ (blue line) as a function of the perturbation wave number \hat{k} for $S = 10^8$, $P_m = 5$ and $C = 2(150)^2$. (b) Corresponding two-dimensional slice of the phase/scenario diagram identifying (1) the Hahm–Kulsrud scenario, (2) the Wang–Bhattacharjee scenario, and (3) our scenario.

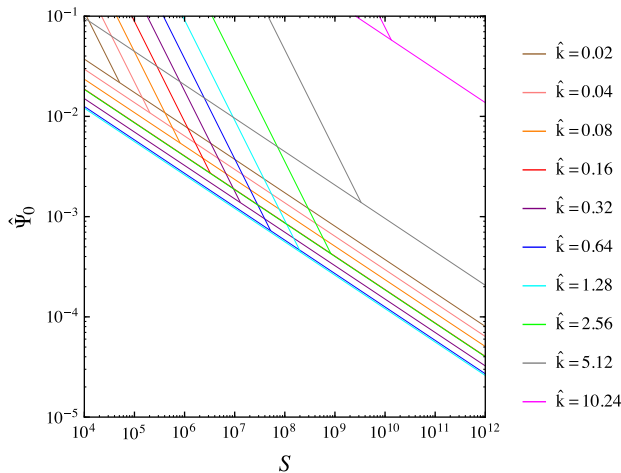


FIGURE 6. Boundaries (identified by the functions $\hat{\Psi}_0 = \hat{\Psi}_W/3$ and $\hat{\Psi}_0 = \hat{\Psi}_c$ for $\hat{\Psi}_c > \hat{\Psi}_W/3$) of the different possible evolutions of the reconnection process for $P_m = 5$ and various values of the perturbation wave number.

The increase of the magnetic Prandtl number extends the domain of existence of the slow reconnection scenario (1) at the expense of the fast reconnection scenario (3). The area of existence of scenario (2) remains almost unchanged, but shifted towards higher values of the Lundquist number.

We now examine in more detail how the possible evolutions of the forced magnetic reconnection process depend on the wave number of the boundary perturbation. Figure 5(a) shows the thresholds $\hat{\Psi}_0 = \hat{\Psi}_W/3$ and $\hat{\Psi}_0 = \hat{\Psi}_c$ as a function of \hat{k} for fixed values of $S = 10^8$ and $P_m = 5$. Below a critical perturbation wave number \hat{k}^* (corresponding to $\hat{k}^* \approx 1$ for the fixed parameters used in figure 5a), every time the

non-constant- ψ magnetic island passes into the nonlinear regime, the evolution of the system leads to the plasmoid-dominated phase predicted in scenario (3). The domains of existence of the possible evolutions (1)–(3) are illustrated in figure 5(b). The scenario discussed by Wang and Bhattacharjee happens only for a small range of $(\hat{\Psi}_0, \hat{k})$ parameters. Note also that scenario (3) is facilitated for $\hat{k} \lesssim \hat{k}^*$, while scenario (1) may occur for large amplitude boundary perturbations if $\hat{k} \gg \hat{k}^*$.

To better evaluate the effects of \hat{k} on the possible evolutions of the reconnection process, we plot in figure 6 the boundaries between scenarios (1)–(3) in a parameter space map $(\hat{\Psi}_0, S)$ (as in figures 2 and 4) for fixed $P_m = 5$ but different values of \hat{k} . The maximum area of existence of scenario (2) occurs for $\hat{k} \sim 1$, while for $\hat{k} \ll 1$ and $\hat{k} \gg 1$, scenario (2) appears for a very limited range of $(\hat{\Psi}_0, \hat{k})$ parameters. Note also that scenario (1) is greatly facilitated in the case of very large perturbation wave numbers ($\hat{k} \gg 1$), while scenario (3) is facilitated by relatively large amplitude perturbations with $\hat{k} \lesssim 1$.

5. Discussion

The introduction of a new type of phase/scenario diagram that explicitly includes the effects of the external drive has allowed us to graphically organize in detail the possible evolutions of forced magnetic reconnection processes in collisional plasmas. In contrast to previous versions of the phase diagrams (Huang *et al.* 2011; Ji & Daughton 2011; Daughton & Roytershteyn 2012; Cassak & Drake 2013; Huang & Bhattacharjee 2013; Karimabadi & Lazarian 2013), this new representation highlights regions of the parameter space $(\hat{\Psi}_0, \hat{k}, S, P_m)$ in which reconnection is a slow diffusive process (§ 3.1), in addition to regions where reconnection can be fast (§§ 3.2 and 3.3). We recall that by fast we mean that the out-of-plane inductive electric field at the X -point is a significant fraction of the one evaluated upstream of the reconnection layer. We also emphasize that this type of diagram responds to the criticism made by Cassak & Drake (2013), concerning the fact that the previously proposed diagrams are not able to take into account the dynamical evolution of the reconnection process from a slow to a fast regime inside a given region of the parameter space. Indeed, scenarios (1)–(3) describe the forced magnetic reconnection process from the current sheet formation all the way to their specific nonlinear evolution.

We would like to remark that while the proposed parameter space diagrams represent a valid way to summarize the current knowledge of the forced magnetic reconnection dynamics in a collisional plasma, there are a number of conditions that may significantly affect the reconnection process but which have not been addressed in this paper. For instance, two-fluid/kinetic effects should be considered if the length scale associated with the width of the reconnecting current sheet becomes of the order of, or smaller than, the characteristic length scales of these effects. In fact, effects associated with finite electron inertia (Ottaviani & Porcelli 1993; Comisso & Asenjo 2014) are known to enhance the reconnection rate, as well as Hall effects (Birn *et al.* 2001; Simakov & Chacón 2008) in antiparallel reconnection (i.e. in the absence of a guide magnetic field) and electron pressure (Kleva *et al.* 1995; Grasso *et al.* 1999) and ion gyration effects (Comisso *et al.* 2013) in the case of reconnection with a strong guide field. We would also like to remark that a common condition in many physical systems is the presence of velocity flows, which are known to suppress the reconnection (Fitzpatrick 1993; Waelbroeck *et al.* 2012) or to alter the reconnection rate (Cassak 2011; Tassi *et al.* 2014). In this case our analysis should be extended

by considering the effects of a plasma flow on the reconnection dynamics. Similarly, the effects of turbulence should also be considered (Servidio *et al.* 2009; Karimabadi & Lazarian 2013) in order to obtain a more complete description of the magnetic reconnection dynamics.

Finally, it is important to recall that all the presented diagrams of magnetic reconnection are based on two-dimensional models and simulations. At present, the knowledge of how magnetic reconnection evolves in large three-dimensional systems is still far behind our understanding of what happens in two-dimensional systems. Therefore, despite the great progress achieved in recent years (Borgogno *et al.* 2005; Yin *et al.* 2008; Daughton *et al.* 2011; Wyper & Pontin 2014), other work is needed in this direction before we can implement a phase diagram description of three-dimensional magnetic reconnection.

Acknowledgements

The authors would like to acknowledge fruitful conversations with R. Fitzpatrick and E. Lazzaro. This work was carried out under the Contract of Association Euratom-ENEA and was also supported by the US Department of Energy under Contract DE-FG02-04ER-54742.

REFERENCES

- ASENJO, F. A. & COMISSO, L. 2015 Generalized magnetofluid connections in relativistic magnetohydrodynamics. *Phys. Rev. Lett.* **114**, 115003.
- AVINASH, K., BULANOV, S. V., ESIRKEPOV, T., KAW, P., PEGORARO, F., SASOROV, P. V. & SEN, A. 1998 Forced magnetic field line reconnection in electron magnetohydrodynamics. *Phys. Plasmas* **5**, 2849.
- BHATTACHARJEE, A. 2004 Impulsive magnetic reconnection in the Earth's magnetotail and the solar corona. *Annu. Rev. Astron. Astrophys.* **42**, 365–384.
- BHATTACHARJEE, A., HUANG, Y.-M., YANG, H. & ROGERS, B. 2009 Fast reconnection in high-Lundquist-number plasmas due to the plasmoid instability. *Phys. Plasmas* **16**, 112102.
- BIAN, N. & VEKSTEIN, G. 2005 Energetics of forced magnetic reconnection in a visco-resistive plasma. *Phys. Plasmas* **12**, 072902.
- BIRN, J., DRAKE, J. F., SHAY, M. A., ROGERS, B. N., DENTON, R. E., HESSE, M., KUZNETSOVA, M., MA, Z. W., BHATTACHARJEE, A., OTTO, A. & PRITCHETT, P. L. 2001 Geospace environmental modeling (GEM) magnetic reconnection challenge. *J. Geophys. Res.* **106**, 3715.
- BIRN, J., GALSGAARD, K., HESSE, M., HOSHINO, M., HUBA, J., LAPENTA, G., PRITCHETT, P. L., SCHINDLER, K., YIN, L., BÜCHNER, J., NEUKIRCH, T. & PRIEST, E. R. 2005 Forced magnetic reconnection. *Geophys. Res. Lett.* **32**, L06105.
- BIRN, J. & HESSE, M. 2007 Reconnection rates in driven magnetic reconnection. *Phys. Plasmas* **14**, 082306.
- BISKAMP, D. 2000 *Magnetic Reconnection in Plasmas*. Cambridge University Press.
- BOOZER, A. H. 2012 Theory of tokamak disruptions. *Phys. Plasmas* **19**, 058101.
- BORGOGNO, D., GRASSO, D., PORCELLI, F., CALIFANO, F., PEGORARO, F. & FARINA, D. 2005 Aspects of three-dimensional magnetic reconnection. *Phys. Plasmas* **12**, 032309.
- CASSAK, P. A., MULLAN, D. J. & SHAY, M. A. 2008 From solar and stellar flares to coronal heating: theory and observations of how magnetic reconnection regulates coronal conditions. *Astrophys. J.* **676**, L69.
- CASSAK, P. A., SHAY, M. A. & DRAKE, J. F. 2009 Scaling of Sweet–Parker reconnection with secondary islands. *Phys. Plasmas* **16**, 120702.
- CASSAK, P. A. 2011 Theory and simulations of the scaling of magnetic reconnection with symmetric shear flow. *Phys. Plasmas* **18**, 072106.

- CASSAK, P. A. & DRAKE, J. F. 2013 On phase diagrams of magnetic reconnection. *Phys. Plasmas* **20**, 061207.
- COLE, A. & FITZPATRICK, R. 2004 Forced magnetic reconnection in the inviscid Taylor problem. *Phys. Plasmas* **11**, 3525.
- COMISSO, L., GRASSO, D., WAELBROECK, F. L. & BORGOGNO, D. 2013 Gyro-induced acceleration of magnetic reconnection. *Phys. Plasmas* **20**, 092118.
- COMISSO, L. & ASENJO, F. A. 2014 Thermal-inertial effects on magnetic reconnection in relativistic pair plasmas. *Phys. Rev. Lett.* **113**, 045001.
- COMISSO, L., GRASSO, D. & WAELBROECK, F. L. 2014 Formation of plasmoid chains in fusion relevant plasmas. *J. Phys.: Conf. Ser.* **561**, 012004.
- COMISSO, L., GRASSO, D. & WAELBROECK, F. L. 2015 Extended theory of the Taylor problem in the plasmoid-unstable regime. *Phys. Plasmas* **22**, 042109.
- DAUGHTON, W., ROYTERSHTEYN, V., KARIMABADI, H., YIN, L., ALBRIGHT, B., BERGEN, B. & BOWERS, K. 2011 Role of electron physics in the development of turbulent magnetic reconnection in collisionless plasmas. *Nature Phys.* **7**, 539–542.
- DAUGHTON, W. & ROYTERSHTEYN, V. 2012 Emerging parameter space map of magnetic reconnection in collisional and kinetic regimes. *Space Sci. Rev.* **172**, 271–282.
- DEWAR, R. L., BHATTACHARJEE, A., KULSRUD, R. M. & WRIGHT, A. M. 2013 Plasmoid solutions of the Hahn–Kulsrud–Taylor equilibrium model. *Phys. Plasmas* **20**, 082103.
- EASTWOOD, J. P., PHAN, T., MOZER, F. S., SHAY, M. A., FUJIMOTO, M., RETINÒ, A., HESSE, M., BALOGH, A., LUCEK, E. A. & DANDOURAS, I. 2007 Multi-point observations of the Hall electromagnetic field and secondary island formation during magnetic reconnection. *J. Geophys. Res.* **112**, 6235.
- FITZPATRICK, R. 1993 Interaction of tearing modes with external structures in cylindrical geometry (plasma). *Nucl. Fusion* **33**, 1049.
- FITZPATRICK, R. 2003 A numerical study of forced magnetic reconnection in the viscous Taylor problem. *Phys. Plasmas* **10**, 2304.
- FITZPATRICK, R., BHATTACHARJEE, A., MA, Z. W. & LINDE, T. 2003 Wave driven magnetic reconnection in the Taylor problem. *Phys. Plasmas* **10**, 4284.
- FITZPATRICK, R. 2004a Scaling of forced magnetic reconnection in the Hall-magnetohydrodynamic Taylor problem. *Phys. Plasmas* **11**, 937.
- FITZPATRICK, R. 2004b Scaling of forced magnetic reconnection in the Hall-magnetohydrodynamical Taylor problem with arbitrary guide field. *Phys. Plasmas* **11**, 3961.
- FITZPATRICK, R. 2008 Scaling of the peak magnetic reconnection rate in the inviscid Taylor problem. *Phys. Plasmas* **15**, 024503.
- GORDOVSKYY, M., BROWNING, P. K. & VEKSTEIN, G. E. 2010a Particle acceleration in a transient magnetic reconnection event. *Astron. Astrophys.* **519**, A21.
- GORDOVSKYY, M., BROWNING, P. K. & VEKSTEIN, G. E. 2010b Particle acceleration in fragmenting periodic reconnecting current sheets in solar flares. *Astrophys. J.* **720**, 1603.
- GRASSO, D., CALIFANO, F., PEGORARO, F. & PORCELLI, F. 1999 Hamiltonian magnetic reconnection. *Plasma Phys. Control. Fusion* **41**, 1497.
- GUO, F., LIU, Y.-H., DAUGHTON, W. & LI, H. 2015 Particle acceleration and plasma dynamics during magnetic reconnection in the magnetically-dominated regime. *Astrophys. J.* **806**, 167.
- HAHM, T. S. & KULSRUD, R. M. 1985 Forced magnetic reconnection. *Phys. Fluids* **28**, 2412.
- HOSSEINPOUR, M. & VEKSTEIN, G. 2008 Collisionless forced magnetic reconnection in an electron–positron plasma. *Phys. Plasmas* **15**, 022904.
- HOSSEINPOUR, M. 2013 The scaling of reconnection rate in the two-fluid model of a collisionless forced magnetic reconnection. *J. Plasma Phys.* **79**, 519–524.
- HUANG, Y.-M. & BHATTACHARJEE, A. 2010 Scaling laws of resistive magnetohydrodynamic reconnection in the high-Lundquist-number, plasmoid-unstable regime. *Phys. Plasmas* **17**, 062104.
- HUANG, Y.-M., BHATTACHARJEE, A. & SULLIVAN, B. P. 2011 Onset of fast reconnection in Hall magnetohydrodynamics mediated by the plasmoid instability. *Phys. Plasmas* **18**, 072109.

- HUANG, Y.-M. & BHATTACHARJEE, A. 2013 Plasmoid instability in high-Lundquist-number magnetic reconnection. *Phys. Plasmas* **20**, 055702.
- JI, H. & DAUGHTON, W. 2011 Phase diagram for magnetic reconnection in heliophysical, astrophysical, and laboratory plasmas. *Phys. Plasmas* **18**, 111207.
- KAGAN, D., SIRONI, L., CERUTTI, B. & GIANNIOS, D. 2015 Relativistic magnetic reconnection in pair plasmas and its astrophysical applications. *Space Sci. Rev.* **186**, 1.
- KARIMABADI, H. & LAZARIAN, A. 2013 Magnetic reconnection in the presence of externally driven and self-generated turbulence. *Phys. Plasmas* **20**, 112102.
- KLEVA, R. G., DRAKE, J. F. & WAELBROECK, F. L. 1995 Fast reconnection in high temperature plasmas. *Phys. Plasmas* **2**, 23.
- LAZZARO, E. & COMISSO, L. 2011 Magnetic reconnection controlled by external current drive. *Plasma Phys. Control. Fusion* **53**, 054012.
- LIN, J. & FORBES, T. G. 2000 Effects of reconnection on the coronal mass ejection process. *J. Geophys. Res.* **105**, 2375.
- LOUREIRO, N. F., SCHEKOCIHIN, A. A. & COWLEY, S. C. 2007 Instability of current sheets and formation of plasmoid chains. *Phys. Plasmas* **14**, 100703.
- LOUREIRO, N. F., SCHEKOCIHIN, A. A. & UZDENSKY, D. A. 2013 Plasmoid and Kelvin–Helmholtz instabilities in Sweet–Parker current sheets. *Phys. Rev. E* **87**, 013102.
- MA, Z. W., WANG, X. & BHATTACHARJEE, A. 1996 Forced magnetic reconnection and the persistence of current sheets in static and rotating plasmas due to a sinusoidal boundary perturbation. *Phys. Plasmas* **3**, 2427.
- MASUDA, S., KOSUGI, T., HARA, H., TSUNETA, S. & OGAWARA, Y. 1994 A loop-top hard X-ray source in a compact solar flare as evidence for magnetic reconnection. *Nature* **371**, 495–497.
- MURPHY, N. A., MIRALLES, M. P., POPE, C. L., RAYMOND, J. C., WINTER, H. D., REEVES, K. K., SEATON, D. B., VAN BALLEGOOIJEN, A. A. & LIN, J. 2012 Asymmetric magnetic reconnection in solar flare and coronal mass ejection current sheets. *Astrophys. J.* **751**, 56.
- NEWCAMB, W. A. 1958 Motion of magnetic lines of force. *Ann. Phys.* **3**, 347–385.
- NICOLAS, T., SABOT, R., GARBET, X., LÜTJENS, H., LUCIANI, J.-F., GUIMARAES-FILHO, Z., DECKER, J. & MERLE, A. 2012 Non-linear magnetohydrodynamic simulations of density evolution in Tore Supra sawtooth plasmas. *Phys. Plasmas* **19**, 112305.
- ØIEROSET, M., PHAN, T. D., FUJIMOTO, M., LIN, R. P. & LEPPING, R. P. 2001 In situ detection of collisionless reconnection in the Earth's magnetotail. *Nature* **412**, 414–417.
- OTTAVIANI, M. & PORCELLI, F. 1993 Nonlinear collisionless magnetic reconnection. *Phys. Rev. Lett.* **71**, 3802.
- PARK, W., MONTICELLO, D. A. & WHITE, R. B. 1984 Reconnection rates of magnetic fields including the effects of viscosity. *Phys. Fluids* **27**, 137.
- PEGORARO, F. 2012 Covariant form of the ideal magnetohydrodynamic ‘connection theorem’ in a relativistic plasma. *Europhys. Lett.* **99**, 35001.
- PORCELLI, F. 1987 Viscous resistive magnetic reconnection. *Phys. Fluids* **30**, 1734.
- PRIEST, E. R., FOLEY, C. R., HEYVAERTS, J., ARBER, T. D., CULHANE, J. L. & ACTON, L. W. 1998 Nature of the heating mechanism for the diffuse solar corona. *Nature* **393**, 545.
- REM, J. & SCHEP, T. J. 1998 Nonlinear dynamics in forced reconnection. *Plasma Phys. Control. Fusion* **40**, 139.
- RUTHERFORD, P. H. 1973 Nonlinear growth of the tearing mode. *Phys. Fluids* **16**, 1903.
- SAMTANEY, R., LOUREIRO, N. F., UZDENSKY, D. A., SCHEKOCIHIN, A. A. & COWLEY, S. C. 2009 Formation of plasmoid chains in magnetic reconnection. *Phys. Rev. Lett.* **103**, 105004.
- SERVIDIO, S., MATTHAEUS, W. H., SHAY, M. A., CASSAK, P. A. & DMITRUK, P. 2009 Magnetic reconnection in two-dimensional magnetohydrodynamic turbulence. *Phys. Rev. Lett.* **102**, 115003.
- SKENDER, M. & LAPENTA, G. 2010 On the instability of a quasiequilibrium current sheet and the onset of impulsive bursty reconnection. *Phys. Plasmas* **17**, 022905.
- SIMAKOV, A. & CHACÓN, L. 2008 Quantitative, comprehensive, analytical model for magnetic reconnection in hall magnetohydrodynamics. *Phys. Rev. Lett.* **101**, 105003.

- SIRONI, L., PETROPOULOU, M. & GIANNIOS, D. 2015 Relativistic jets shine through shocks or magnetic reconnection? *Mon. Not. R. Astron. Soc.* **450**, 183–191.
- SU, Y., VERONIG, A. M., HOLMAN, G. D., DENNIS, B. R., WANG, T., TEMMER, M. & GAN, W. 2013 Imaging coronal magnetic-field reconnection in a solar flare. *Nat. Phys.* **9**, 489–493.
- TASSI, E., GRASSO, D. & COMISSO, L. 2014 Linear stability analysis of collisionless reconnection in the presence of an equilibrium flow aligned with the guide field. *Eur. Phys. J. D* **68**, 88.
- TENERANI, A., RAPPAZZO, A. F., VELLI, M. & PUCCI, F. 2015 The tearing mode instability of thin current sheets: the transition to fast reconnection in the presence of viscosity. *Astrophys. J.* **801**, 145.
- VALORI, G., GRASSO, D. & DE BLANK, H. J. 2000 Collisionless reconnection in instabilities and due to external forcing. *Phys. Plasmas* **7**, 178.
- VEKSTEIN, G. & BIAN, N. 2006 Hall assisted forced magnetic reconnection. *Phys. Plasmas* **13**, 122105.
- WADDELL, B. V., CARRERAS, B., HICKS, H. R., HOLMES, J. A. & LEE, D. K. 1978 Mechanism for major disruptions in tokamaks. *Phys. Rev. Lett.* **41**, 1386.
- WAELEBROECK, F. L. 1989 Current sheets and nonlinear growth of the $m = 1$ kink-tearing mode. *Phys. Fluids B* **1**, 2372.
- WAELEBROECK, F. L., JOSEPH, I., NARDON, E., BÉCOULET, M. & FITZPATRICK, R. 2012 Role of singular layers in the plasma response to resonant magnetic perturbations. *Nucl. Fusion* **52**, 074004.
- WANG, X. & BHATTACHARJEE, A. 1992a Forced reconnection and current sheet formation in Taylor's model. *Phys. Fluids B* **4**, 1795.
- WANG, X. & BHATTACHARJEE, A. 1992b Forced reconnection, current sheets, and coronal heating. *Astrophys. J.* **401**, 371.
- WYPER, P. F. & PONTIN, D. I. 2014 Non-linear tearing of 3D null point current sheets. *Phys. Plasmas* **21**, 082114.
- YAMADA, M., LEVINTON, F. M., POMPHREY, N., BUDNY, R., MANICKAM, J. & NAGAYAMA, Y. 1994 Investigation of magnetic reconnection during a sawtooth crash in a high-temperature tokamak plasma. *Phys. Plasmas* **1**, 3269.
- YAMADA, M. 2011 Mechanisms of impulsive magnetic reconnection: global and local aspects. *Phys. Plasmas* **18**, 111212.
- YIN, L., DAUGHTON, W., KARIMABADI, H., ALBRIGHT, B. J., BOWERS, K. J. & MARGULIES, J. 2008 Three-dimensional dynamics of collisionless magnetic reconnection in large-scale pair plasmas. *Phys. Rev. Lett.* **101**, 125001.